

Atmospheric-pressure large-area DBDs in Ar-HMDSO: experiments and 1D fluid modelling

C.-P. Klages¹, M. M. Becker², J. Schäfer², D. Hegemann³, B. Nisol⁴, S. Watson⁴, M. R. Wertheimer⁴, D. Loffhagen²

¹TU Braunschweig, Institute for Surface Technology, Bienroder Weg 54, 38108 Braunschweig, Germany

²Leibniz Institute for Plasma Science and Technology, Felix-Hausdorff-Str. 2, 17489 Greifswald, Germany

³EMPA, Swiss Federal Laboratories for Materials Science and Technology, Plasma & Coating Group, Lerchenfeldstr. 5, 9014 St. Gallen, Switzerland

⁴Groupe des Couches Minces (GCM) and Department of Engineering Physics, Polytechnique Montréal, Montréal QC, Canada H3C 3A7

Abstract: Numerical calculations employing a spatially one-dimensional (1D) fluid-Poisson model and electrical measurements are applied to analyse the electrical discharge characteristics of a large experimental dielectric barrier discharge in Ar-HMDSO mixtures containing up to 600 ppm of the monomer. Reasonable agreement between electrical measurements and modelling results is generally found. Differences between the measured and calculated electrical energy dissipated in the plasma per period are still under discussion.

Keywords: dielectric barrier discharge, HMDSO, plasma polymerization, modelling

1. Introduction

Since many decades hexamethyldisiloxane (HMDSO) has been used as prototype precursor (“monomer”) for plasma deposition of organosilicon thin films under low-pressure conditions or at atmospheric pressure employing dielectric barrier discharges (DBDs) [1]. A numerical study of DBDs in argon with small admixtures of HMDSO (mole fractions $x \leq 300$ ppm) using a time-dependent, spatially one-dimensional fluid-Poisson model was published recently [2]. A plane-parallel discharge configuration with rectangular electrodes having a width of 8 cm and a length (in gas flow direction) of only 1 cm, and a discharge gap of 1 mm was analysed in this work. The reason for choosing such unusually short electrodes in the experiments [3] and the model was to keep the residence time and plasma-chemical conversion of the monomer during its passage through the plasma zone small.

Considering 22 reactions of HMDSO with electrons, excited Ar atoms and molecules, and atomic and molecular Ar ions in the reaction kinetics model, the fluid model calculations were able to reproduce several discharge characteristics reasonably well, such as the temporal evolution of the discharge current for several values of x as well as the measured substantial decrease of the ignition voltage and the dissipated power at constant applied voltage with growing x . The electron production was found to be dominated by Penning ionization due to energy transfer from metastable and resonant excited Ar atoms (Ar^*) to HMDSO molecules above $x \approx 5$ ppm. The production of neutral trimethylsilyl (TMS^\cdot) and trimethylsiloxy (TMS-O^\cdot) radicals, main precursors of the deposited film, also takes place largely due to collision processes of HMDSO with Ar^* as well as Ar_2^* excimers, followed by dissociation.

A drawback of the electrode configuration with 1 cm length is the relatively large effect of electrode edges and the fringing electric field, making a precise electrical characterization difficult. For this reason, the present

contribution reports on experimental results obtained for a DBD reactor of larger area in section 2 and on corresponding numerical calculations employing the same model as in [2] in section 3. HMDSO mole fractions x up to 1500 ppm were used in the experiments, while the numerical studies covered the range of $0 < x/\text{ppm} \leq 600$.

2. Experimental results

The large-area DBD reactor (two electrodes, 6 cm length and 18 cm width each, total discharge area 216 cm^2) used for plasma-polymerization experiments with HMDSO monomer (also referred to as “dopant” in the 10 slm Ar carrier gas flow) reported here is shown in Fig. 1.

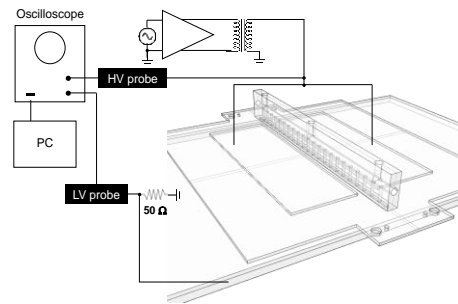


Fig. 1. Schematic drawing of the atmospheric-pressure DBD plasma reactor used for plasma polymerization experiments.

The methodology used for determining values of the electrical energy dissipated per period E_g and $\Delta E_g(F_d) = E_{\text{Ar}}(0) - E_{\text{Ar}}(F_d)$ as functions of the monomer flow F_d (in sccm) was described in detail earlier [4]. Figs. 2 and 3 present plots of E_g and ΔE_g .

The “plateau” in ΔE_g versus F_d has not only been observed for HMDSO but also for several other plasma polymerization (PP) monomers examined so far (see e.g. [4]). In [5] we reported gradients in PP-HMDSO coating composition in the flow direction at least for small F_d

values up to 1.2 sccm corresponding to $x = 120$ ppm. At the same time the coatings were found to be chemically uniform in the monomer-rich region at higher flow rates (see $F_d = 6$ sccm corresponding to $x = 600$ ppm for example), which correspond to the “plateau” in ΔE_g .

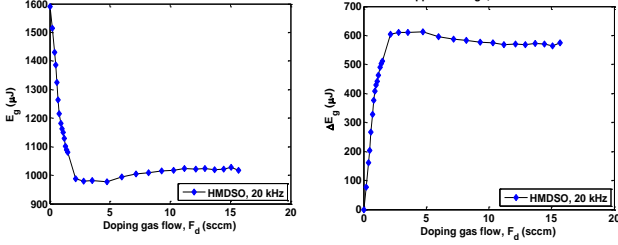


Fig. 2. (left) and Fig. 3. (right) Plots of E_g and ΔE_g , respectively, as function of the dopant gas flow in 10 slm of Ar carrier gas in a 20 kHz DBD plasma with constant applied voltage amplitude $V_{a,amp} = 4$ kV.

3. Results of numerical modelling

Figure 4 shows the equivalent circuit which was used to analyse the measured electrical data and determine the gap voltage V_{gap} as well as the gas current I_g and discharge current I_d .

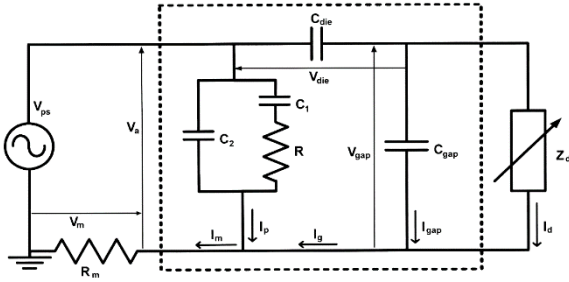


Fig. 4. Equivalent electrical circuit diagram, where the portion in the dashed rectangle represents the discharge cell. $R_m = 50 \Omega$; for other details, see ref. [6].

Figure 5 shows a selection of results representing the temporal discharge behaviour for two selected values of x , 200 and 600 ppm, respectively.

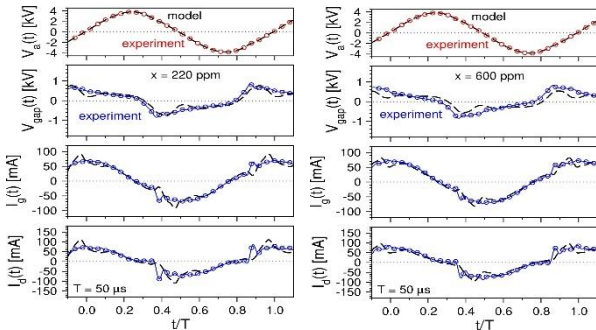


Fig. 5. Temporal evolution of applied and gap voltages V_a and V_{gap} , respectively, gas current I_g and discharge current I_d for one period ($50 \mu s$). Model results: black dashed line, measured or experimental input quantities: blue or red data points and lines, respectively.

In general, there is reasonable agreement between gap voltages and currents resulting from model calculations and data derived from the electrical measurements and related equivalent-circuit analysis.

Root mean square (rms) values of experimental gap voltage and currents are virtually constant for $x \geq 150$ ppm, while the modelling results decrease continuously, as shown in Figs. 6 and 7.

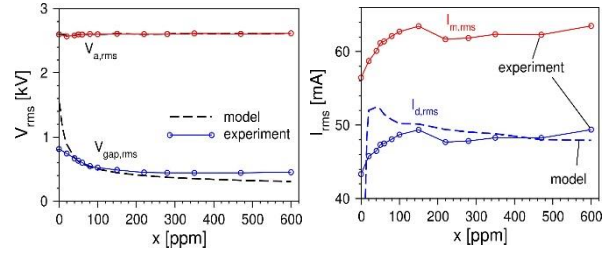


Fig. 6. (left) and Fig. 7. (right) Comparison of model results with experimental data: rms gap and applied voltages (left), rms discharge and measured currents (right).

Below $x \approx 150$ ppm, the measured rms discharge current $I_{d,rms}$ increases with increasing x by roughly 6%, while $V_{gap,rms}$ decreases by about 35%. The integral of the product $I_d(t) \cdot V_{gap}(t)$ over one period, representing the energy dissipated within one period E_g , shows a substantial decrease both in model calculations and in the experiment, see Fig. 8.

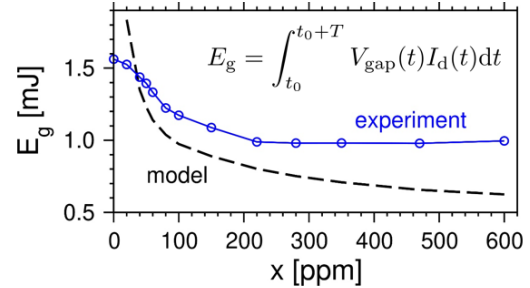


Fig. 8. Energy dissipated per period in the DBD: modelling vs. experimental results.

While the fluid modelling results show a monotone decrease of E_g with increasing x , the measured E_g becomes virtually constant for $x \geq 220$ ppm (cf. Fig. 2).

The following two figures 9 and 10 allow an insight into the major channels leading to ionization in the Ar-HMDSO mixtures with different monomer mole fractions x (Fig. 9) as well as into the contributions $P_m(x)$ of individual plasma-chemical processes involving the monomer HMDSO to the total dissipation of electrical energy (Fig. 10). Figure 9 shows a slow decrease of the total ionization rate with increasing x . Penning ionization by reactions of HMDSO with excited Ar atoms dominates over the whole range of mole fractions. The contribution of direct HMDSO ionization by electron collisions increases up to

about 18% at $x = 600$ ppm while the corresponding process is completely negligible for ground-state Ar atoms.

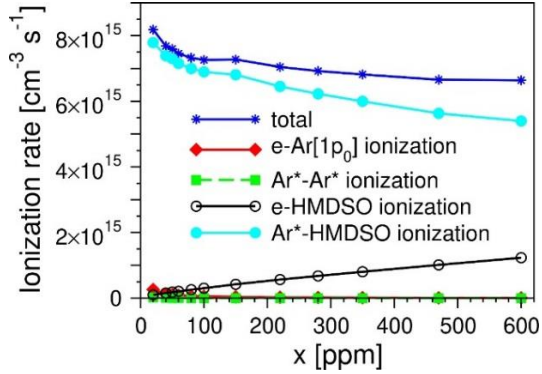


Fig. 9. Average ionization rates as functions of x .

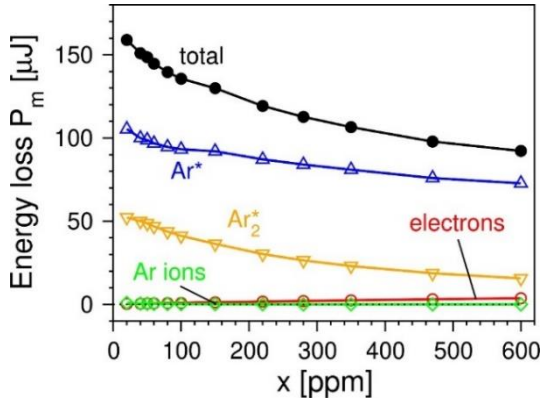


Fig. 10. Energy losses due to HMDSO collisions as functions of x .

The contributions of different collision processes involving HMDSO are shown in Fig. 10, together with the sum of these contributions. In contrast to the situation in low-pressure plasmas, the triplet excimer Ar_2^* , formed by three-body collisions of $Ar(1s_5)$ atoms with two ground-state Ar atoms, contributes substantially, in addition to Ar atoms in metastable or resonant states, summarized as “ Ar^* ”. Owing to its fast reaction to Ar_2^* , $Ar(1s_5)$ itself has a negligible share in reactions with HMDSO, while atoms in the resonant state $Ar(1s_2)$ begin to dominate beyond $x \approx 100$ ppm, because they have the highest generation rate of all Ar^* atoms [7].

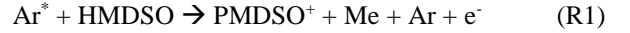
4. Discussion

Aside from HMDSO, a large number of monomers has been studied experimentally in a similar manner as it is described here exemplarily. Corresponding results can be found in a series of papers (see [8] and references therein). Using the observed decrease of the measured electrical energy dissipated per period

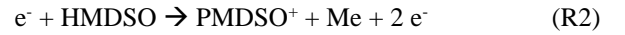
$$\Delta E_g(F_d) = E_{Ar}(0) - E_{Ar}(F_d), \quad (1)$$

a quantity E_m was calculated by dividing $\Delta E_g(F_d)$ by the number of monomer molecules passing the discharge zone per period, where a monomer flow $F_d = 1$ sccm corresponds to an inflow of $4.48 \cdot 10^{17}$ molecules/s. The obtained values of E_m , representing the dissipated electrical energy per molecule, depend on F_d (or x) going to zero for large F_d in the monomer-rich region and covering a range up to about 100 eV/molecule. E_m was discussed in terms of energy consumption due to plasma-chemical dissociation of the monomers.

The numerical calculations demonstrate the prominent role played by energy transfer reactions from excited Ar atoms (Ar^*) and molecules (Ar_2^*) for the production of electrons beyond about 20 ppm monomer mole fraction. The ionization is virtually exclusively due to dissociative Penning ionization processes



up to $x \approx 100$ ppm, while the direct ionization of HMDSO

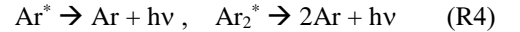


is comparably less important. Here $PMDSO^+$ denotes the pentamethylsiloxanyl ion and Me is the methyl radical.

Parallel with Penning ionization processes, the dissociation of HMDSO due to collisions with Ar^* according to



and the corresponding processes with Ar_2^* take place. In addition, atoms in resonant states (and excimers) can lose their energy by radiation processes



A comparison with measured ignition voltages shows that the ratio of the reaction rates of (R1) and (R3), defined as $\alpha/(1-\alpha)$ is about 0.3/0.7, i.e., about 30% of the collisions $Ar^* + HMDSO$ lead to ionization due to Penning processes [2].

Experimentally these processes results in a substantial decrease of the ignition voltage V_i to about 1/3 of the value $V_i(x=0)$ in [2] as well as of the rms gap voltage by $\approx 55\%$ (cf. Figure 6) in the present study. The reason for these effects is that a lower reduced field is required to get a given ionization rate via collisions of HMDSO with excited atoms Ar^* having threshold energies of 11.5 eV at least than due to direct electron-impact ionization of Ar requiring more than 15.8 eV.

The decrease of dissipated power or energy per period E_g is also mainly caused by the impact of the Penning ionization processes and the resulting drop of the ignition and gap voltages. In [2], the decline of E_g starts steeply for

$x \leq 10$ ppm and becomes progressively smaller for a larger HMDSO admixture, when the competing reactions (R4) become less and less important.

If less dissociation processes (R3) into neutral fragments would take place, corresponding to $\alpha > 30\%$, more Ar^* atoms were available for ionization reactions (R1) resulting in an even larger drop of the ignition voltage and dissipated power [2].

Here, it should be mentioned that the Manley equation [9] derived for filamented ozonizer DBDs with a near constant gap voltage in the “active phase” cannot be used to calculate the dissipated power in the present case for larger x because the DBD in Ar-HMDSO mixtures turns into a glow discharge at monomer fractions beyond $x \approx 20$ ppm. The Manley equation would predict an increase of the power with growing x . In fact, such an effect could be observed in the still filamented regime for very small monomer mole fraction ($x \approx 1$ ppm) in a DBD arrangement with a 1 mm gas gap. However, the power as well as the ignition voltage generally decreased for monomers such as HMDSO, hexamethylcyclotrisiloxane and octamethylcyclotetrasiloxane for $x > 5$ ppm [10].

A final comment should be made concerning the sharp bending of the measured curves E_g and ΔE_g towards a virtual concentration independence beyond mole fractions of about 200 ppm ($F_d > 2$ sccm) in Figs. 2 and 3, respectively, suggesting that the gas phase becomes sort of “saturated” with HMDSO. This behaviour is at variance with results of the numerical calculations showing a monotonous decrease of E_g at least up to $x = 600$ ppm (cf. Fig. 8) parallel to a declining rms gap voltage (Fig. 6). The decrease of $V_{g,rms}$ may be due to an increasing role by direct electron-impact ionization of HMDSO reaction (R2) requiring only about 9 eV electron energy, even less than the generation of Ar^* states (11.5 eV)

One may speculate that the concentration of monomers in the gas phase stays unchanged with a further increase of HMDSO flow in the experiment due to the formation of nanoparticulate HMDSO polymers consuming a growing amount of the monomers. This effect is not considered in the numerical model. In fact, the formation of nanoparticles in DBDs in Ar-HMDSO and Ar-C₂H₂ has been reported in the literature [11]. The discharges ran under conditions similar to those used here or in [3]. The particles were collected from the gas phase as far as 50 cm downstream from the plasma for 1000 to 2000 ppm acetylene and 145 ppm HMDSO, respectively. Deposition of films with milky appearance behind the plasma zone composed of particles of 50 to 100 nm in size was also observed in the experiments reported in [3] for HMDSO mole fractions larger than about 70 ppm.

By inspection of the deposit, there was no evidence that nanoparticles were actually formed in the experiments

reported in the present paper. In order to arrive at a clarification of the reasons for the differences between the modelling and experimental results shown in Figure 8, it would be very interesting to investigate to what extent the surplus HMDSO leaves the DBD reactor unchanged and as nanoparticulate polymers, respectively, using gas-phase infrared spectroscopy or mass spectrometry and a nanoparticle-collection method.

5. References

- [1] R. Foest, F. Adler, F. Sigeneger, M. Schmidt, *Surf. Coat. Technol.* **163–164**, 323 (2003).
- [2] D. Loffhagen, M. M. Becker, A. K. Czerny, J. Philipp, C.-P. Klages, *Contrib. Plasma Phys.* **58**, 337 (2018).
- [3] J. Philipp, A. K. Czerny, C.-P. Klages, *Plasma Process. Polym.* **13**, 509 (2016).
- [4] B. Nisol, H. Gagnon, S. Lerouge, M. R. Wertheimer *Plasma Process. Polym.* **13**, 366 (2016).
- [5] D. Hegemann, B. Nisol, S. Watson, M. R. Wertheimer, *Plasma Chem. Plasma Process* **37**, 257 (2017).
- [6] M. Archambault-Caron, H. Gagnon, B. Nisol, K. Piyakis, M. R. Wertheimer, *Plasma Sources Sci. Technol.* **24**, 045004 (2015).
- [7] C.-P. Klages, A. K. Czerny, J. Philipp, M. M. Becker, D. Loffhagen, *Plasma Process Polym.* **14**, e1700081 (2017).
- [8] B. Nisol, S. Watson, A. Meunier, D. Juncker, S. Lerouge, M. R. Wertheimer, *Plasma Process Polym.* **15**, e1700132 (2018).
- [9] U. Kogelschatz, *Advanced ozone generation, in: Process Technologies for Water Treatment*, Plenum Press, New York (1988).
- [10] J. Philipp, A. K. Czerny, C.-P. Klages, unpublished.
- [11] V. Vons, Y. Creyghton, A. Schmidt-Ott, *J. Nanoparticle Res.* **8**, 721 (2006).